



## SWIFT-XRT-CALDB-04

Release Date: March 13<sup>th</sup>, 2013

Prepared by: Claudio Pagani, Andrew Beardmore, Tony Abbey (UL), Matteo Perri, Milvia Capalbi (ASDC)

Date revised: February 9<sup>th</sup>, 2013

Revision: 12

Revised by: Claudio Pagani & Andy Beardmore

# SWIFT-XRT CALDB RELEASE NOTE

## SWIFT-XRT-CALDB-04: Gain

### 1 Component Files

Table 1: Latest CALDB component files.

FILENAME	VALID DATE	RELEASE DATE	REVISION
swxpcgains6_20010101v012.fits <sup>a</sup>	01-Jan-2001	13-Mar-2013	12
swxwtgains6_20010101v013.fits <sup>a</sup>	01-Jan-2001	13-Mar-2013	12
swxpcgains0_20010101v011.fits <sup>b</sup>	01-Jan-2001	13-Mar-2013	12
swxwtgains0_20010101v012.fits <sup>b</sup>	01-Jan-2001	13-Mar-2013	12

<sup>a</sup> 's6' refers to  $V_{ss} = 6$  V gain files. The substrate voltage was raised permanently to this value on 2007-Aug-30 at 14:25UT.

<sup>b</sup> 's0' refers to substrate voltage ( $V_{ss}$ ) 0 V gain files.

## 2 Introduction

This document contains a description of the analysis performed at Leicester University to produce the gain calibration products for the *Swift*-XRT Calibration Database (CALDB).

Section 3 introduces the modifications to the gain files in this release. Section 4 summarizes the changes in the *Swift* operations during the mission that had a significant impact on the gain characterisation, such as the substrate voltage change and the charge traps analysis and corrections, and the modifications to the gain files and software to account for these changes. Section 5 describes the updates in this release and the quality of the new gain files. Appendix A illustrates the derivation of the gain and CTI coefficients and their implementation in the CALDB gain files; in Appendix B the gain and CTI measurements are described; the charge traps analysis is shown in Appendix C; Appendix D lists the previous gain file releases.

## 3 Updates in current Gain Files release (revision 12)

Two sets of gain files are released in this CALDB update, for substrate voltage  $V_{ss} = 6\text{ V}$  and  $V_{ss} = 0\text{ V}$  respectively: **swxpcgains6\_20010101v012.fits** for Photon Counting mode and **swxwtgains6\_20010101v013.fits** for Windowed Timing mode are the  $V_{ss} = 6\text{ V}$  gain files; **swxpcgains0\_20010101v011.fits** for PC mode and **swxwtgains0\_20010101v012.fits** for WT mode are the  $V_{ss} = 0\text{ V}$  gain files. The substrate voltage was raised permanently to  $V_{ss} = 6\text{ V}$  on 2007-Aug-30 at 14:25UT.

The following updates to the  $V_{ss} = 6\text{ V}$  gain files are included in this release:

- New gain and CTI coefficients from the analysis of the corner source data during 2012;
- New charge trap correction tables from Tycho calibration data in February and August-September 2012;
- Modelling of the temperature dependence of the trap corrections included in the gain files.

Radiation damage is causing the degradation of the CCD spectral response; updates to the gain and CTI coefficients and the charge trap table corrections maintain the accuracy of the gain energy scale and partially recover the spectral resolution (the improvement of the FWHM in calibration observations is reported in tables 2 and 3). As discussed in Section 5, residual energy offsets of  $\sim 10\text{ eV}$  can be seen at energies  $\sim 2\text{ keV}$  where charge trap corrections are derived, while the energy scale is accurate to within  $\sim 30\text{ eV}$  at energies close to the Iron line ( $6.4\text{ keV}$ ). The details of the analysis of the temperature dependence of the charge trap corrections and its implementation in the current gain files release is described in Section 5. The previous version of the gain files (revision 11) was released on February 9th of 2012 and included updates to the gain and CTI coefficients and to the trap tables up to September 2011 and the implementation of a broken power law to model the CTI energy dependence.

We also make available updated  $V_{ss} = 0\text{ V}$  gain files, for use with data up to 2007-Aug-30 (i.e. before the substrate voltage changed). The files contain modified offset coefficient (the terms GC3, GC3.TRAP), for both PC and WT mode, in order to make them compatible with new  $V_{ss} = 0\text{ V}$  RMFs also released with this XRT CALDB update.

## 4 Review of Gain File Changes

### 4.1 Passive cooling and Substrate Voltage change

The loss of the CCD active cooling system shortly after launch forced the instrument to rely on passive cooling provided by the XRT radiator in order to operate the detector in the  $-75^{\circ}\text{C}$  to  $-50^{\circ}\text{C}$  temperature range rather than the  $-100^{\circ}\text{C}$  envisaged before launch. The main effects of operating at such temperatures is a change of gain and a significant level of dark current and elevated CCD noise at low energies, with an increasing number of hot and ‘flickering’ pixels at higher temperatures.

On 2007-Aug-30 at 14:25UT, the XRT team performed a planned substrate voltage ( $V_{ss}$ ) change from 0V to 6V in order to reduce the thermally induced dark current when the operating temperature is above  $-55^{\circ}\text{C}$ . Prior to the change, preliminary observations of Cas A and the Crab at a  $V_{ss}$  of 6V showed a reduction in the Quantum Efficiency of the order of 10% at 6 keV (Godet et al. 2007, SPIE, 6686) and an increase of about 5% in the gain due to the change in the gain of the output FET. The latter meant separate gain files are needed depending on the substrate voltage at the time of a given observation. The files are distinguished using the notation *s0* (for  $V_{ss} = 0\text{V}$ ) and *s6* (for  $V_{ss} = 6\text{V}$ ) in their respective file names. The *Swift* software tools (version 2.3 and onwards) were updated to perform a query for the relevant gain file to be used depending on the substrate voltage setting.

### 4.2 Radiation damage

Radiation damage during the orbital lifetime of *Swift* continues to degrade the XRT CCD camera performance. The interaction of soft and hard protons with the CCD produces displacements of Silicon atoms that cause charge traps in its crystal lattice, resulting in offsets in the measured photons energies and in the broadening of the spectroscopic resolution.

In September of 2007 the XRT team started a calibration program to characterise the charge losses due to traps consisting of observations of the emission line rich Cas A and Tycho Supernova Remnants (SNRs). In Photon Counting (PC) mode, the locations of the deeper traps and their depths are measured in the central 200x200 pixels of the CCD. Outside the central window, the cumulative effects of traps are evaluated for individual CCD column. Column energy offsets are also evaluated in Windowed Timing (WT) mode, that provides high time resolution with 1-D spatial localisation. The observations of the SNRs are repeated approximately every six months, and updated trap tables are derived. The CALDB gain files in this release have been updated including trap tables from 2 additional epochs (February and August-September 2012) as derived from observations of the Tycho SNR. The temperature dependence of the trap depths was also characterized and updated gain coefficients were included in this release.

The XRTCALCPI software task implements the energy corrections for charge traps and the CTI energy dependence. The software automatically applies the appropriate gain corrections dependent on the time of observation, CCD temperature and event position. The trap mapping analysis is described in Appendix C.

### 4.3 Calibration corner source analysis and CTI energy dependence

In 2008 June, after successful XRT flight software updates, the XRT CCD began permanently operating in full frame PC mode ('pcw3'), whereby the entire  $600 \times 600$  imaging area of the CCD is read out. This has enabled us to continuously collect corner source  $^{55}\text{Fe}$  calibration data (see figure A.1) when operating in PC mode and has provided us with a wealth of information on the gain and charge transfer efficiency (CTE) behaviour as a function of time and CCD temperature since this time.

Moreover, analysis of the corner source data and measurements of the nickel background line in addition to the Tycho, Cas A and E0101 SNR lines has clearly shown that the CTI correction should be energy dependent. The energy dependence (coefficients GC1, GC2 and GC1\_TRAP, GC2\_TRAP of the gain files) has been calibrated and modelled with a broken power law and implemented in the XRTDAS software version 2.8.0 and onwards. The 'Calibration Dataset Codename', used by the software to query the CALDB has been set to 'GAIN2' in the gain files with the new CTI energy dependence:

```
CCNM0001= 'GAIN2 ' / Type of Calibration data
```

This setting prevents the software from using an incorrect version of the gain files.

## 5 Gain file derivation and accuracy of the energy scale

### 5.1 Introduction

The gain files include coefficients for the gain and the parallel and serial CTI for different epochs at three reference CCD temperatures (-75C, -61.5C and -48C). The gain coefficients are defined in Appendix A. The coefficients are derived using the  $^{55}\text{Fe}$  line in the corner sources spectra at different epochs (Appendix B). Two sets of gain and CTI coefficients are included in the gain files for this release. One set of coefficients, derived from all the events in the corner sources, is used by the software to calculate the event energy when no trap correction is applied. The second set, derived from the columns of the corner sources less affected by charge traps, is used when the traps energy corrections are applied. The CTI energy dependence is modelled with a broken power-law functional form (Appendix A.6).

The gain files format allows for the energy correction for charge trap losses. The traps are identified in the gain files by their locations in detector coordinates (RAWX, RAWY), their extensions in pixels (YEXTENT) and their depths in eV (OFFSET) measured at the incident photons reference energy of 1.856 keV (the observed Tycho Silicon  $K\alpha$  energy). Starting with the release HEASOFT 6.11, the *Swift* software derives the trap corrected energy and saves it in the *PI* column of the cleaned events files for each valid X-ray event. The user can optionally store in the column *PLNOM* the energies of the X-ray events derived without trap corrections by setting the parameter *savepinom* to 'yes'.

In the current release the parameters used to model the temperature dependence of the trap depths have been included in the PC gain file (Section 5.2). The new coefficients provide improved fits of the emission lines of the Tycho and Cas A SNRs and the instrumental Nickel  $K\alpha$  over the CCD operating temperatures ( $\sim$ -70C to  $\sim$ -50C).

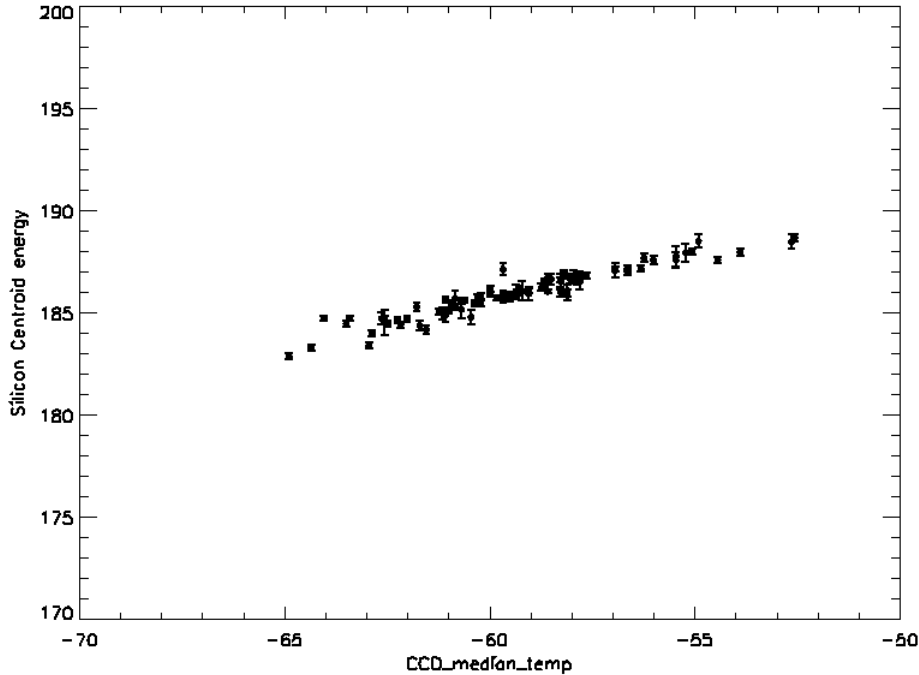


Figure 1: The effect of the temperature dependence of the trap depths as seen in Tycho observations taken in October of 2010, with the Silicon line centroid energy plotted as a function of the CCD operating temperature. When the CCD is warmer the thermal noise fills the traps, resulting in a shift to higher measured energies of the X-ray events.

PC trap corrected spectra extracted using the new version 12 of the PC gain file (`swxpc-gains6_20010101v012.fits`) should be fitted with the PC RMF+ARF version 13 (`swxpc0to12s6_20010101v013.rmf` and `swxpc0s6_20010101v013.rmf`, `swxpc0to12s6_20010101v013.arf` and `swxpc0s6_20010101v013.arf`). Windowed Timing trap corrected spectra extracted using the new version 13 of the WT gain file (`swxwtgains6_20010101v013.fits`) should be fitted with the WT RMF+ARF version 14 (`swxwt0to2s6_20010101v014.rmf` and `swxwt0s6_20010101v014.rmf`, `swxwt0to2s6_20010101v014.arf` and `swxwt0s6_20010101v014.arf`).

## 5.2 Trap corrections temperature dependence

The trap depths are temperature dependent because at higher CCD operating temperatures the dark current fills the traps. This behaviour can be seen, for example, from the corner sources analysis, where the high statistics allow the measurements of depth of individual traps at different temperatures, and can be observed in the long trap mapping Tycho observations in PC mode (Figure 1). In WT mode observations the effect is not seen because of the continuous and faster charge readout mode.

To model the observed temperature dependence we utilized the instrumental Nickel  $K\alpha$  line at 7.47 keV, by analysing every PC mode observation with an exposure time greater than 100 seconds. The data were processed merging all the observations taken during a year, removing point sources and extracting spectra selecting operating CCD temperatures with bins of 1 degree and by fitting the measured Nickel line energy. The results of this procedure can be seen for

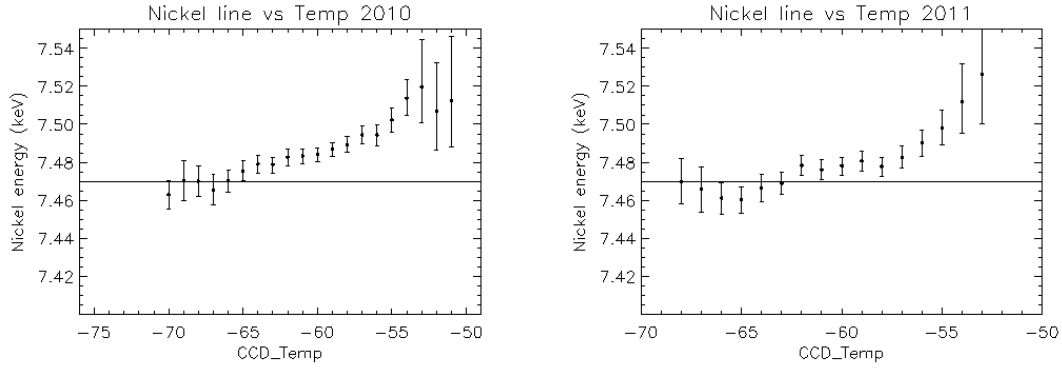


Figure 2: The Nickel line in PC data from years 2010 (left panel) and 2011 (right panel) show evidence of energy shifts from the expected values as a function of temperature.

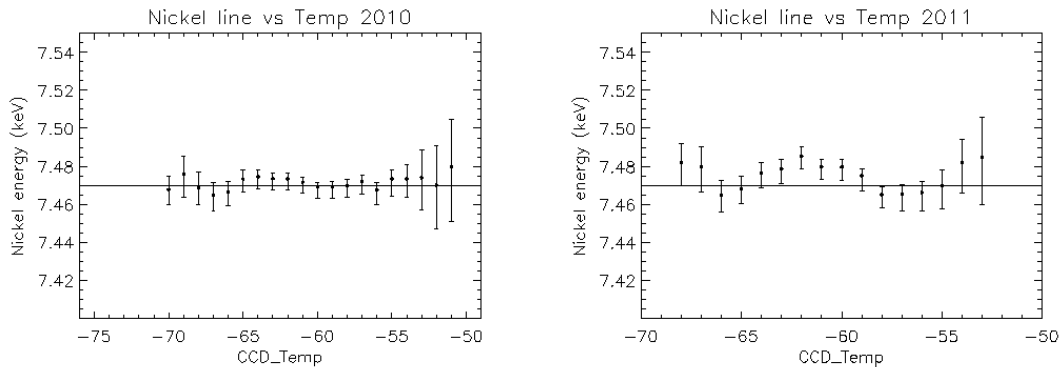


Figure 3: Processing the PC data with the updated gain file, that includes temperature dependent trap tables, the gaussian fit to the Nickel line gives energies close to the expected value at all temperatures, as can be seen in the analysis of the observations taken in 2010 (left panel) and 2011 (right panel).

example for observations taken during 2010 and 2011 (Figure 2).

The energy shifts from the expected Nickel line energy were measured and are included in the gain files as GC3\_TRAP coefficients at the reference temperatures of -75C, -61.5C and -48C for the 2010 epochs. The XRTCALPI software task applies a linear interpolation of the GC3\_TRAP coefficients to derive the energy offset correction at all CCD temperatures. For the 2011 and 2012 epochs, a non linearity of the temperature dependence is seen for CCD temperatures above -55C in the Nickel line analysis and the best modelling and correction of the temperature dependence was obtained by including distinct offsets trap tables at the reference temperatures of -75C, -61.5C and -48C in the gain files. The results of the applied corrections for the 2011 dataset can be seen in the right panel of Figure 3.

### 5.3 Quality of the new gain files

This release includes gain files with updated trap measurements from the two most recent calibration epochs, February and August-September 2012. These new Tycho observations and the analysis of the corner source data showed a slow, gradual increase of the radiation damage

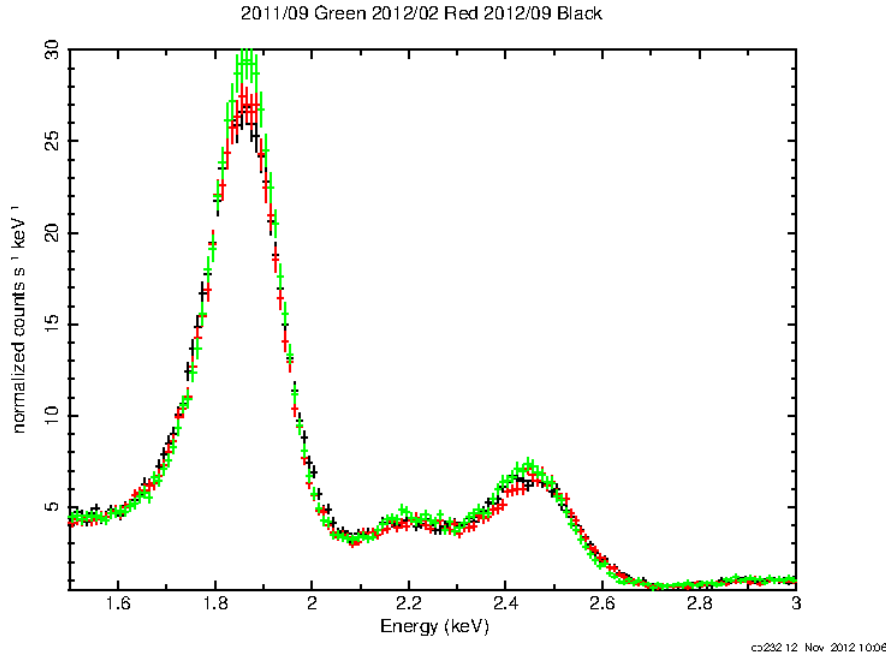


Figure 4: Trap corrected spectra of the Tycho SNR from observations taken in September 2011 (black), February 2012 (red) and September 2012 (green). Trap corrections from different epochs continue to provide a substantial recovery of the emission line flux and of the energy resolution.

since previous epochs. Figure 4 shows Tycho trap corrected spectra extracted in September 2011 (black), February 2012 (red) and September 2012 (green). As the radiation damage accumulates over the years with new traps developing, the spectral response is gradually degrading, but trap corrections applied over different epochs continue to provide a substantial recovery in flux and resolution, as summarized in tables 2 and 3 for calibration observations of Cas A and Tycho of different epochs. Recent spectra are shown in Figure 5. Trap corrected data (in red) clearly improve the resolution of the observed spectra. The emission lines are better defined in PC observations (left panel) as the energy corrections are applied for individual deep traps, while in WT mode (right panel) the energies are corrected for each column.

With the previous release the characterisation of the energy dependence of the trap depths was improved by modelling the CTI with a broken power law. In particular, the then newly derived break energy and the power law indices in WT mode provide more accurate energy centroids at the Sulfur and Iron lines in Cas A and Tycho and lower energy lines in E0102.

The analysis of the Nickel line provides a quality and efficacy check of the new gain file, as it tests trap energy corrections for observations at different epochs and at a different energy from the Silicon line used in the Tycho trap mapping calibrations. The satisfactory result can be seen for example in Figure 6 from all PC observations taken in 2012, that shows the Nickel line of the trap corrected data at the expected energy and with a recovery in the line flux and resolution compared to the observed spectrum.

Some limitations remain in the current release. The accuracy of the trap mapping measurements in PC mode data is dependent on the statistics of the reference Silicon  $K\alpha$  line, and only traps with a depth greater than 20 eV can be identified; the effects of shallower traps are included in the general CTI description. Outside the central 200x200 pixel window columns energy offsets are used to correct the data, but deep traps can cause energy shifts that remain unaccounted

Table 2: PC spectral resolution: Full width half maximum (FWHM) in eV of the Silicon, Sulfur and Iron  $K\alpha$  lines of the observed and the corrected spectra at different calibration epochs (specified as YYYY/MM). The FWHM values at Sulfur and Iron are only reported when enough counts in the lines allow for a reliable fit.

Source	Epoch	Line	$FWHM_{observed}$	$FWHM_{corrected}$
CasA	2007/09	Si	$138 \pm 7$	$114 \pm 2$
		S	$200 \pm 11$	$146 \pm 6$
		Fe	$318 \pm 22$	$286 \pm 21$
CasA	2009/02	Si	$154 \pm 8$	$122 \pm 2$
		S	$251 \pm 18$	$163 \pm 7$
		Fe	$372 \pm 25$	$321 \pm 14$
Tycho	2009/10	Si	$179 \pm 8$	$132 \pm 3$
		S	$267 \pm 14$	$182 \pm 8$
		Fe	$381 \pm 45$	$299 \pm 31$
Tycho	2010/03	Si	$177 \pm 7$	$138 \pm 3$
		S	$256 \pm 10$	$184 \pm 8$
		Fe	$381 \pm 39$	$307 \pm 32$
Tycho	2010/10	Si	$192 \pm 7$	$139 \pm 7$
		S	$269 \pm 11$	$192 \pm 11$
		Fe	$387 \pm 34$	$304 \pm 27$
Tycho	2011/02	Si	$185 \pm 6$	$143 \pm 7$
Tycho	2011/09	Si	$191 \pm 7$	$147 \pm 7$
Tycho	2012/02	Si	$191 \pm 7$	$146 \pm 7$
Tycho	2012/09	Si	$198 \pm 8$	$149 \pm 7$

Table 3: WT spectral resolution: Full width half maximum (FWHM) in eV of the Silicon, Sulfur and Iron  $K\alpha$  in the observed and the the corrected spectra for different calibration epochs (specified as YYYY/MM). The FWHM values at Sulfur and Iron are only reported when enough counts in the lines allow for a reliable fit.

Source	Epoch	Line	$FWHM_{observed}$	$FWHM_{corrected}$
CasA	2007/10	Si	$152 \pm 13$	$106 \pm 3$
		S	$244 \pm 15$	$138 \pm 7$
		Fe	$383 \pm 16$	$304 \pm 15$
CasA	2008/07	Si	$157 \pm 14$	$113 \pm 4$
		S	$274 \pm 17$	$154 \pm 9$
		Fe	$393 \pm 22$	$325 \pm 17$
CasA	2009/10	Si	$212 \pm 16$	$120 \pm 3$
		S	$302 \pm 11$	$170 \pm 11$
Tycho	2009/11	Si	$222 \pm 15$	$136 \pm 7$
Tycho	2010/10	Si	$238 \pm 12$	$148 \pm 5$
Tycho	2011/02	Si	$234 \pm 11$	$150 \pm 6$
Tycho	2011/08	Si	$234 \pm 12$	$154 \pm 6$
Tycho	2012/02	Si	$243 \pm 12$	$160 \pm 7$
Tycho	2012/08	Si	$249 \pm 12$	$166 \pm 7$



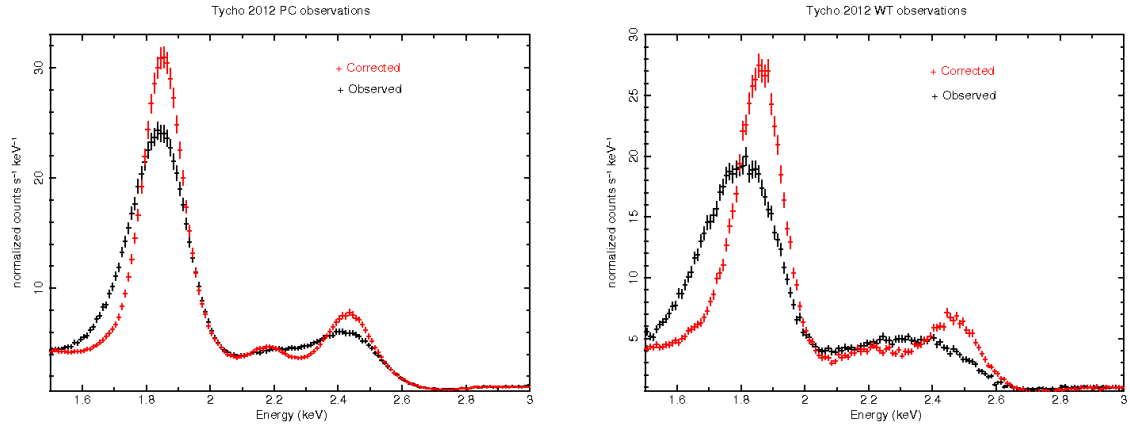


Figure 5: Comparison of observed spectra (in black) and trap corrected spectra (in red) in recent 2012 Tycho observations. The recovery in PC observations (left panel) yields better defined emission lines as energy corrections are applied for each deep trap, while in WT observations (right panel) a single energy offset is applied for all X-ray events in a column.

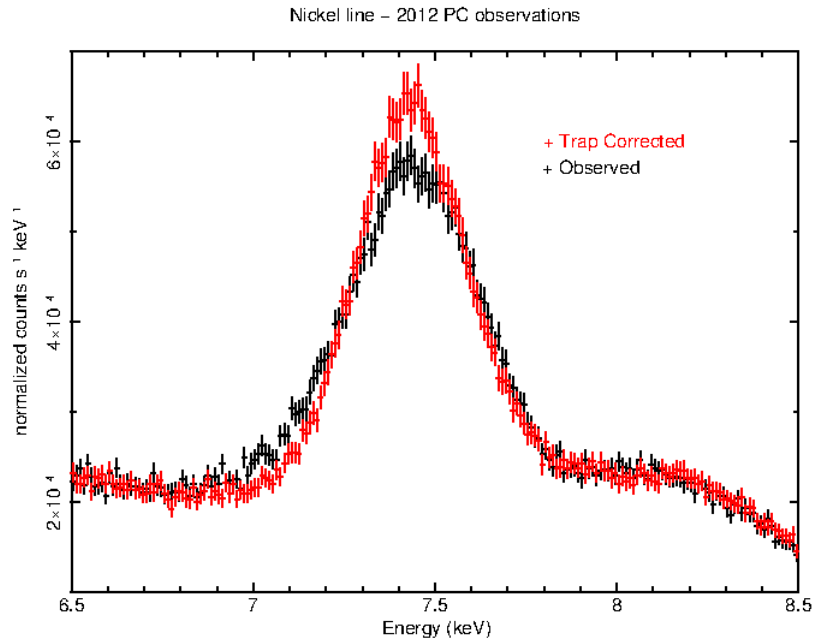


Figure 6: Nickel line extracted from all 2012 PC observations with exposure greater than 100 seconds. The trap corrected spectrum (in red) shows a recovery of the line flux and an improvement of the energy resolution in comparison to the observed spectrum (in black).

for because their row position is not known. In WT mode observations, traps are not mapped individually, and only the cumulative energy offsets of each column is measured and corrected. Finally, in between releases of updated gain files new traps caused by radiation damage will develop that can cause shifts in the measured energies that depend on the observed source positions on the detector.

Because of the mentioned limitations and the pixel-specific nature of the distribution of traps on the detector a general description of the accuracy of the XRT energy scale for this gain file calibration release is not straightforward. We estimate the accuracy by fitting short observa-

tions of the Cas A SNR taken months after the trap-mapping calibration epochs using XMM derived models. When the line energies are left as free parameters of the fit differences of less than 10 eV from the XMM values are measured in the PC spectrum, while in WT mode the differences can be higher, up to 30 eV at Iron  $K\alpha$ .

## APPENDIX

### A Gain and CTI coefficients

#### A.1 Introduction

The charge transfer efficiency ( $CTE$ ) is defined as the fractional charge lost per pixel during the charge transfer process. So after  $N$  transfers the remaining charge  $Q$  is

$$Q = Q_o(CTE)^N \quad (\text{A.1})$$

where  $Q_o$  is the initial charge. Or in terms of charge transfer inefficiency  $CTI = 1 - CTE$  this is just

$$Q = Q_o(1 - CTI)^N \quad (\text{A.2})$$

#### A.2 Event energy measured in the SWIFT-XRT CCD22

A schematic of the *Swift*-XRT CCD22 is showed in figure A.1. When an incident X-ray of energy  $E$  is registered as an event at a detector position  $(X, Y)$  in the image section it suffers charge loss from  $Y$  transfers in the parallel direction through the image section, from  $Y_S = 600$  transfers in the parallel direction through the frame-store section and from  $X + 5$  transfers in the serial direction through the readout register (+5 as there are 5 additional pixels at the end of the readout register).  $CTI$  values differ in the parallel and serial direction because of the different transfer times and pixel sizes. In order to describe the total charge lost effectively we need separate  $CTI$  coefficients for the parallel transfer losses incurred in the image and frame-store sections ( $CTI_{p,i}$  and  $CTI_{p,f}$ , respectively, as the physical volume of the pixels are smaller in the latter compared with the former) and another for the serial transfer losses ( $CTI_s$ ).

The event is registered by the ADC as a pulse-height analysed digital number  $D$  (i.e. the  $PHA$  value) according to the following:

$$D = \frac{E}{A}(1 - CTI_{p,i})^Y(1 - CTI_{p,f})^{Y_S}(1 - CTI_s)^{(X+5)} \quad (\text{A.3})$$

Or rearranging slightly, this becomes

$$\begin{aligned} D &= E \left[ \frac{(1 - CTI_{p,f})^{Y_S}(1 - CTI_s)^5}{A} \right] (1 - CTI_{p,i})^Y (1 - CTI_s)^X \\ &= \frac{E}{A'} (1 - CTI_{p,i})^Y (1 - CTI_s)^X \end{aligned} \quad (\text{A.4})$$

where  $A' = A/((1 - CTI_{p,f})^{Y_S}(1 - CTI_s)^5)$  is the system gain.

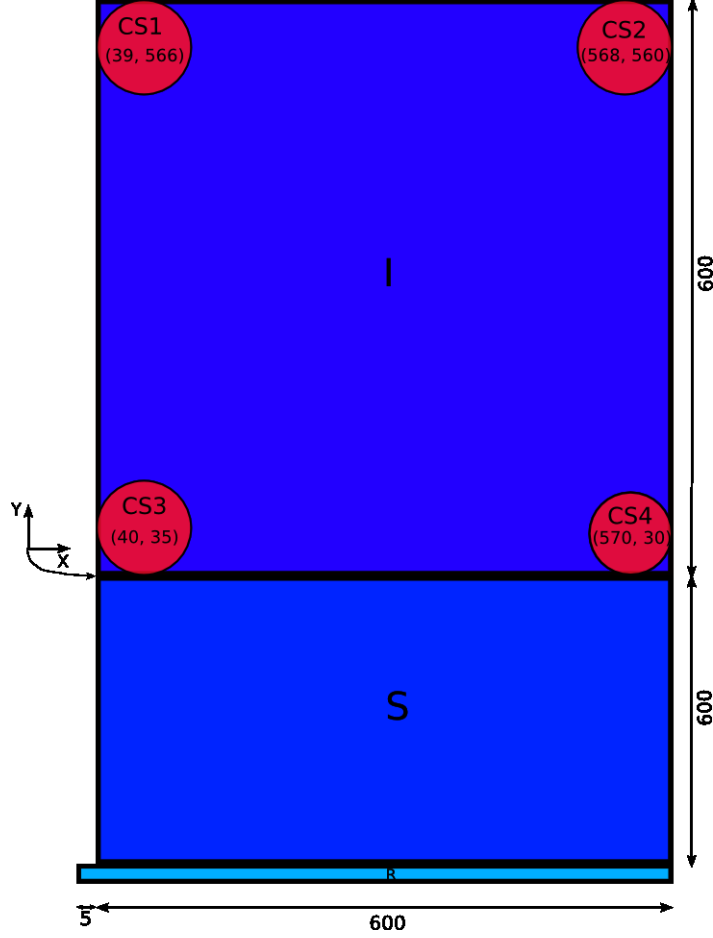


Figure A.1: Schematic of the *Swift*-XRT CCD22 identifying the imaging (I) and frame-store (S) sections, the readout register (R), and the  $^{55}\text{Fe}$  corner sources (CS). Charged is clocked in the parallel direction (Y), through both the imaging and frame-store sections, which have charge transfer inefficiencies  $CTI_{p,i}$  and  $CTI_{p,f}$ , respectively, and in the serial direction through the readout register with  $CTI_s$ .

### A.3 CTI coefficients

The parallel CTI can be determined from CS3 and CS1 by using equation A.4 to construct the ratio  $(D_3 - D_1)/D_3$ , where  $D_n$  are the measured  $^{55}\text{Fe}$  central energies (in DN) for source  $n = 1 \dots 4$ , which is

$$\begin{aligned} \frac{D_3 - D_1}{D_3} &= \frac{(1 - CTI_{p,i})^{Y_3}(1 - CTI_s)^{X_3} - (1 - CTI_{p,i})^{Y_1}(1 - CTI_s)^{X_1}}{(1 - CTI_{p,i})^{Y_3}(1 - CTI_s)^{X_3}} \\ &= 1 - (1 - CTI_{p,i})^{(Y_1 - Y_3)}(1 - CTI_s)^{(X_1 - X_3)} \end{aligned} \quad (\text{A.5})$$

$$= 1 - (1 - CTI_{p,i})^{(Y_1 - Y_3)} \quad (\text{A.6})$$

where equation A.6 is a simplification assuming  $X_1 \approx X_3$  for transfers dominating in the parallel direction (i.e.  $Y_1 - Y_3 \gg X_1 - X_3$ ). Rearranging we find

$$CTI_{p,i} = 1 - \left(\frac{D_1}{D_3}\right)^{1/(Y_1 - Y_3)} \quad (\text{A.7})$$

We often make use of the small number approximation (i.e.  $(1+x)^n \approx 1+nx$ ) so equation A.6 becomes

$$\frac{D_3 - D_1}{D_3} = (Y_1 - Y_3)CTI_{p,i}$$

That is, the parallel CTI is

$$CTI_{p,i} = \frac{D_3 - D_1}{D_3(Y_1 - Y_3)} \quad (\text{A.8})$$

A similar equation can be derived for the parallel CTI derived from CS4 and CS2.

Likewise, the serial CTI can be shown to be

$$CTI_s = 1 - \left(\frac{D_4}{D_3}\right)^{1/(X_4 - X_3)} \quad (\text{A.9})$$

$$= \frac{D_3 - D_4}{D_3(X_4 - X_3)} \quad (\text{A.10})$$

## A.4 Gain

We can obtain the gain  $A'$  from CS3, which is the corner source closest to the output amplifier,

$$A' = \frac{E_{55\text{Fe}}}{D_3} (1 - CTI_{p,i})^{Y_3} (1 - CTI_s)^{X_3} \quad (\text{A.11})$$

where  $E_{55\text{Fe}} = 5895.45$  eV,  $X_3 = 40$  and  $Y_3 = 35$ . Note the term  $(1 - CTI_{p,i})^{Y_3} (1 - CTI_s)^{X_3}$  which provides a small correction to the simple gain estimate of  $E_{55\text{Fe}}/D_3$  and ensures the event energy is calculated relative to the origin (0, 0) of the imaging section of the CCD.

## A.5 Comparison with the CALDB gain file

The CALDB gain file defines the *PHA* channel to *PI* channel conversion as

$$PI \times G = PHA (GC0 + X \times GC1 + Y \times GC2) + GC3 + X \times GC4 + Y \times GC5 \quad (\text{A.12})$$

where  $GCn$  are the gain file coefficients (which are interpolated over time and CCD temperature), and  $G = 10$  eV is the nominal gain.

Equation A.4 can be rearranged to give the event energy from the measured DN value, assuming the *CTI* coefficients are known,

$$E = A' D (1 - CTI_{p,i})^{-Y} (1 - CTI_s)^{-X}. \quad (\text{A.13})$$

Note, this is the exact form of the equation required to reconstruct the event energy from the measure DN value, knowing the gain ( $A'$ ) and *CTI* values.

This equation can be made to resemble the CALDB formula by using the small value approximation expansion :

$$\begin{aligned} E &= A' D (1 + Y CTI_{p,i}) (1 + X CTI_s) \\ &= A' D (1 + X CTI_s + Y CTI_{p,i} + X Y CTI_s CTI_{p,i}) \end{aligned}$$

and dropping the last negligibly small term to give

$$\begin{aligned} E &= A' D (1 + X CTI_s + Y CTI_{p,i}) \\ &= D \{A' + X (A' CTI_s) + Y (A' CTI_{p,i})\}. \end{aligned} \quad (\text{A.14})$$

By comparison with equation A.12, we see that

$$\begin{aligned} GC0 &= A' \\ GC1 &= A' CTI_s \\ GC2 &= A' CTI_{p,i} \end{aligned} \quad (\text{A.15})$$

In practise,  $CTI_s$  is estimated from corner sources CS3–CS4, while  $CTI_{p,i}$  is estimated as the average parallel CTI from corner sources CS1–CS3 and CS2–CS4.

The term  $GC3$  in equation A.12 represents an offset (in eV) associated with the readout electronics.

## A.6 CTI coefficients energy dependence

Laboratory experiments and various X-ray missions (e.g. Chandra, Suzaku) indicate that CTI is energy dependent. We choose to implement an energy dependent CTI correction as a broken power law with index  $\beta_1$  and  $\beta_2$  below and above the break energy:

$$\begin{aligned} CTI(E) &= CTI(E_{55\text{Fe}}) \left(\frac{E}{E_{55\text{Fe}}}\right)^{-\beta_1} & (E \leq E_{55\text{Fe}}) \\ &= CTI(E_{55\text{Fe}}) \left(\frac{E}{E_{55\text{Fe}}}\right)^{-\beta_2} & (E > E_{55\text{Fe}}) \end{aligned} \quad (\text{A.16})$$

with  $E_{55\text{Fe}} = 5.895$  keV and  $\beta > 0$ .

The CTI energy dependence parameters in the CALDB gain files are labelled as BETA1, BETA2 and E\_CTI.

## A.7 Trap correction coefficients

The trap corrections are implemented in the gain files using an additive offset coefficient to equation A.12:

$$PI \times G = PHA (GC0 + X \times GC1 + Y \times GC2) + GC3 + X \times GC4 + Y \times GC5 + OFFSET \quad (\text{A.17})$$

The OFFSET coefficient is added to the  $PI \times G$  values of events detected at specific CCD locations affected by charge traps. In the gain files, the trap positions are labelled as RAWX,

RAWY and YEXTENT, such that the OFFSET PI value will be added to events along the CCD column RAWX between rows RAWY and RAWY+YEXTENT.

The trap offset energy dependence is modelled with a broken power law, with the break at the reference energy of 1.856 keV (the energy of the Silicon K $\alpha$  line of the Tycho SNR):

$$\begin{aligned} \text{Offset}(E) &= \text{Offset}(E_{\text{break}}) \left( \frac{E}{E_{\text{break}}} \right)^{\alpha_1} & (E \leq E_{\text{break}}) \\ &= \text{Offset}(E_{\text{break}}) \left( \frac{E}{E_{\text{break}}} \right)^{\alpha_2} & (E > E_{\text{break}}) \end{aligned} \quad (\text{A.18})$$

The offsets energy dependence parameters in the CALDB gain files are labelled as ALPHA1, ALPHA2 and EBREAK. The gain and CTI coefficients and the energy dependence parameters used by the software to compute trap corrected events energy are labelled as GC0\_TRAP, GC1\_TRAP, GC2\_TRAP, GC3\_TRAP, GC4\_TRAP, GC5\_TRAP, BETA1\_TRAP, BETA2\_TRAP and E\_CTL\_TRAP.

## B Gain and CTI measurements

### B.1 Corner source data analysis

Gain and CTI coefficients are measured from the analysis of the corner source data. A first set of coefficients is derived using the entire dataset, and characterises the CCD response when trap energy corrections are not applied. A second set of coefficients, derived from corner source data least affected by traps, models the gain and the CTI of trap-corrected spectra. For both derivations, the same procedure is applied and is described below.

The corner source are processed applying the PC mode bias corrections. Grade 0 PHA spectra are extracted from each of the corner sources as a function of time and CCD temperature. The spectra near the  $^{55}\text{Fe}$  line are then fit with the following asymmetric Gaussian function :

$$\begin{aligned} G(x) &= N \exp \left( -0.5 \left( \frac{x - x_c}{\sigma_1} \right)^2 \right) & (x < x_c) \\ &= N \exp \left( -0.5 \left( \frac{x - x_c}{\sigma_2} \right)^2 \right) & (x > x_c) \end{aligned}$$

where  $x_c$  is the line centre,  $\sigma_1$  the line width for  $x < x_c$ ,  $\sigma_2$  the line width for  $x > x_c$ , and  $N$  the normalisation. This models the line profile better and returns more accurate line centroids than a simple Gaussian, as the effect of CTI is to broaden the low energy line wing significantly more than the high energy line wing (Godet et al. 2009, A&A, 494, 775).

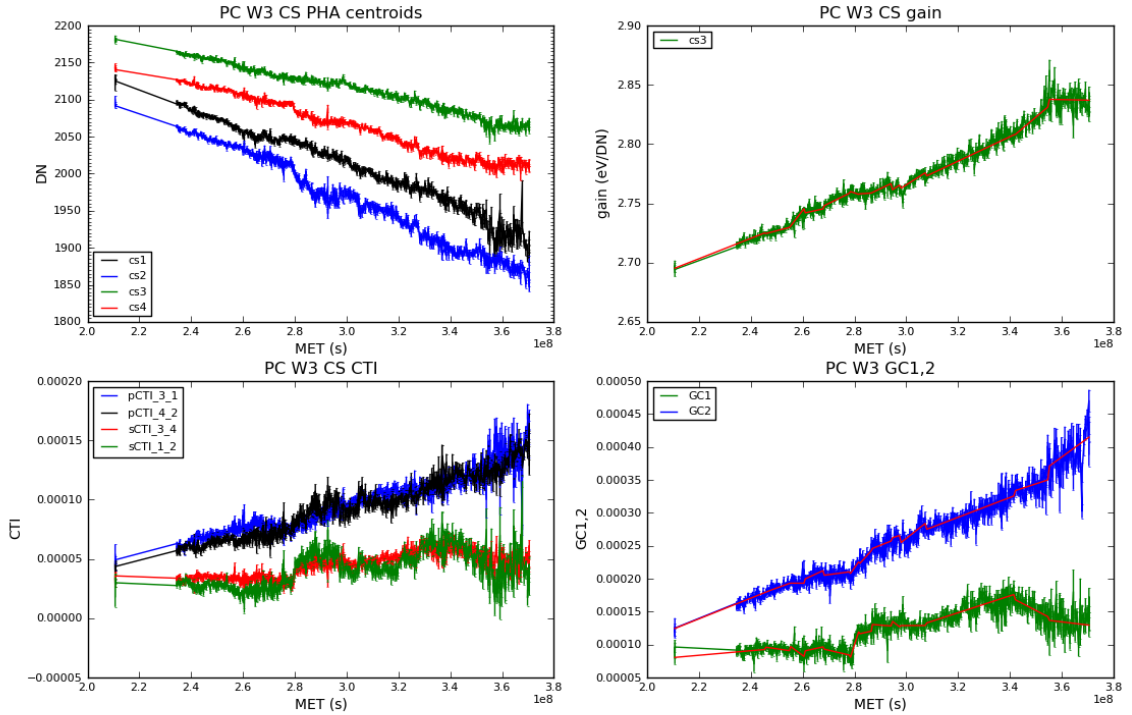


Figure B.2: *Swift*-XRT CCD gain and CTI measurements from the corner source data at a CCD temperature of  $-60^{\circ}\text{C}$  from 2007-Sep-05 to 2012-Sept-30. No trap-correction has been applied to the data. The top-left panel shows the measured  $^{55}\text{Fe}$  line centroids. The top-right panel shows the gain coefficient ( $GC0$ ) estimated using equation A.11. The bottom-left panel shows the measured CTI coefficients for the 4 pairs of corner sources. The bottom-right panel shows the estimated gain file  $GC1$  (serial) and  $GC2$  (parallel) coefficients. (Error bars are  $1\sigma$  estimates.)

### B.1.1 Gain and CTI coefficients for non trap-corrected spectra

Figure B.2 illustrates the measured line centroids, gain and CTI coefficients from 2007-Sep-05 to 2012-Sep-30 at a CCD temperature of  $-60^{\circ}\text{C}$  when all the corner source data is used (i.e., without excluding traps).

Due to the excellent quantity and statistical quality of the corner source data obtained since 2008-June we have been able to study and quantify the measured gain and CTI coefficients behaviour as a function of time and CCD temperature. Figure B.3 shows the gain ( $GC0$ ) and CTI coefficients ( $GC1,2$ ) derived from the entire corner source dataset, plotted as a function of CCD temperature at 4 representative epochs. The data reveal the gain has evolved to become less sensitive to the CCD temperature, while the parallel CTI decreases with increasing temperature and the serial CTI increases slightly with temperature.

We have parameterised the gain and CTI time ( $t$ ) and CCD temperature ( $T$ ) dependence using the following functional form :

$$z(t, T) = a + bt + cT + dt^2 + eT^2 + ftT.$$

The model curves are shown plotted with the data in figure B.3.

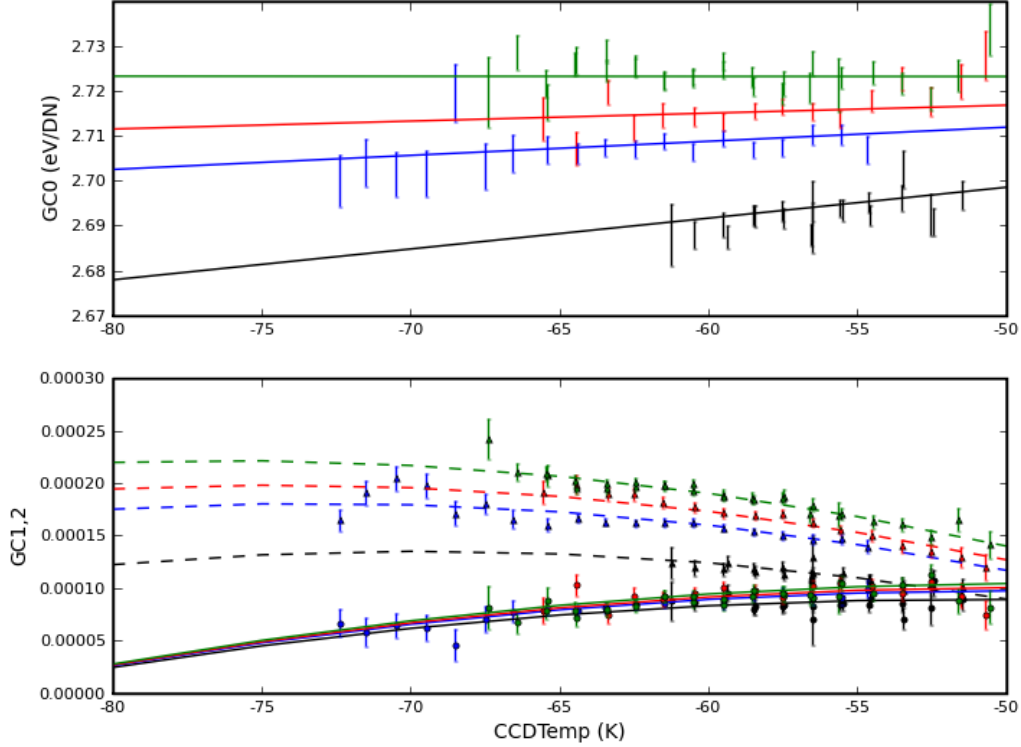


Figure B.3: *Swift*-XRT CCD gain (GC0) and CTI (GC1,2) coefficients plotted against CCD temperature. The model described in the text is over-plotted as the curved lines. For both panels the colour coding is as follows: black – 2007-Sep-06; blue – 2008-Jun-07; red – 2008-Sep-15; green – 2008-Jan-25. In the lower panel, the GC1 (serial) values are drawn as circles and the model is represented by the solid curves, while the GC2 (parallel) values are drawn as triangles and the model curves are shown dashed.

The parameterised GC0, GC1 and GC2 (see equation A.12) values derived from non trap-corrected data were then converted into a template gain file with coefficients calculated at monthly intervals and at three discrete temperatures ( $-73$ ,  $-60.5$ ,  $-48^{\circ}\text{C}$ ). The *Swift*-XRT software task XRTCALPI interpolates over time and temperature when applying the gain calculation to the event data.

The template gain file for non trap-corrected data was tested on various data sets which included the corner source data (PC mode) and the line rich SNRs E0102 and Cas A (both PC and WT mode). The low energy spectrum of SNR E0102, in particular, is sensitive to the presence of residual offsets in the energy scale. This is due to the presence of traps that causes energy offsets of the observed energies.

PC mode calibration observations of E0102 taken between 2007 to 2012 revealed the need for an additional offset for non trap-corrected spectra. The offset is modelled as a function of time with a linear fit and included in the gain file as the GC3 coefficient. At present, we have no independent measure of the CTI characterisation in WT mode so we use the PC mode CTI coefficients in the construction of the WT gain file. Like PC mode, we checked the residual offset using observations of E0102 taken between 2007 and 2012. These showed an average offset of 40 eV valid for all epochs and included as the GC3 coefficient in the gain files.



### B.1.2 Gain and CTI coefficients for trap-corrected spectra

The analysis of the corner source data have revealed an ever increasing number of deep traps (20 eV or deeper) in the XRT camera. Because these deep traps were not excluded from the corner source analysis, the gain and CTI coefficients measured as described above are representative of a CCD response with no trap corrections applied and are labelled in the gain files as GC0, GC1, GC2 and GC3.

To characterise the gain and the CTI of trap-corrected spectra a subset of the corner source columns was selected. As the energy offsets of the deeper traps ( $> 20$  eV) are corrected by the software the gain and the residual CTI is best described by the columns least affected by traps. In particular, the columns within 50 eV of the highest measured  $^{55}\text{Fe}$  energy centroid in the bottom left corner source (DETX = 13, 17, 22, 41) were used to derive the gain coefficient. For the parallel CTI, the accepted columns had a centroid difference in the top and the bottom corner sources within  $\pm 2$  PI channels ( $\pm 25$  eV) of each other: DETX = 6, 9, 13, 20, 23, 31, 36, 47, 57, 67, 68, 69 on the left side of the CCD; DETX = 539, 542, 548, 550, 558, 574, 578, 588, 596, 598 on the right side of the CCD. As already mentioned, the serial CTI for trap corrected spectra is set to zero in the CALDB files, as global energy offsets for each CCD column are instead measured and included in the gain file; for this same reason, GC3\_TRAP is also zero in the gain files.

The coefficients used by the software task XRTCALPI when the trap correction is applied are labelled as GC0\_TRAP, GC1\_TRAP, GC2\_TRAP and GC3\_TRAP. The coefficients are parametrised as a function of time and CCD temperature with the same functional form used for the gain and CTI coefficients of uncorrected spectra previously described. The gain (GC0\_TRAP) and parallel CTI (GC2\_TRAP) measurements as a function of time at the CCD temperature of  $\sim -60\text{C}$  are shown in figure B.4.

## C Trap mapping

The extreme *Swift* environment, and in particular the transits through the South Atlantic Anomaly, have caused a substantial degradation of the CCD performance, mostly due to the creation of charge traps. Figure C.5 shows the comparison of the Cas A SNR spectrum at launch and in an uncorrected observation taken in 2010. The energy degradation is severe, causing the broadening of the brighter lines and the disappearance of the weaker ones.

The initial approach in dealing with the spectral degradation had been the application of a broadening function to the original spectral response. Using this technique the XRT team generated and released RMFs<sup>a</sup> with a redistribution function which matches the broadened response kernel of the detector at any time. As the spectral resolution continued to worsen, this temporary fix was replaced by the better approach of mapping the locations and depths of the traps and correcting the event data for the energy losses incurred. The benefit of this method is that it can restore the spectral resolution of the CCD to something approaching its value at

<sup>a</sup>Two sets of WT and PC RMFs including an epoch-dependent broadened kernel have been released: the first set should be used for data collected from 2007 March 1 to 2007 August 31 (`swxpc0to12s0_20070301v011.rmf` & `swxpc0s0_20070301v011.rmf` for PC mode and `swxwt0s0_20070301v011.rmf` & `swxwt0to2s0_20070301v011.rmf` for WT mode) the second set from 2007 September 01 onwards (`swxpc0to12s6_20070901v011.rmf` & `swxpc0s6_20070901v011.rmf` for PC mode and `swxwt0s6_20070901v012.rmf` & `swxwt0to2s6_20070901v012.rmf` for WT mode)

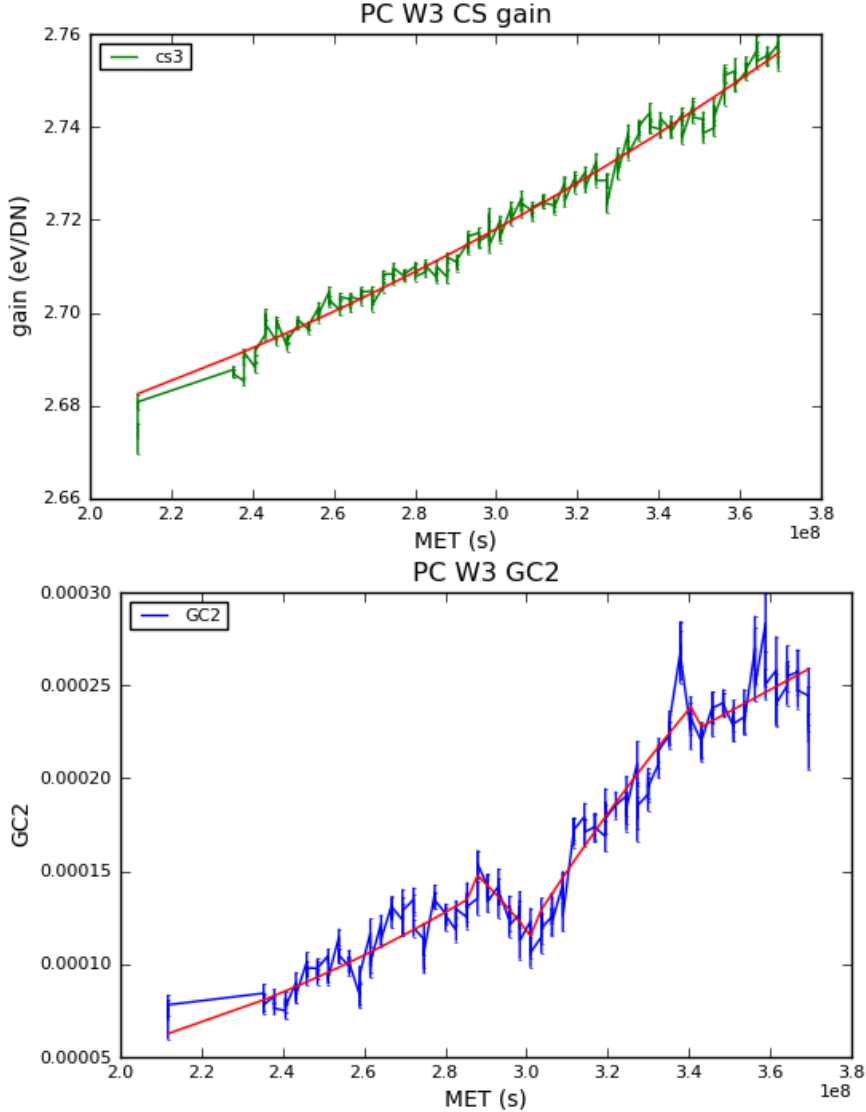


Figure B.4: Gain and parallel CTI coefficients from the subsample of events of the corner source data least affected by trap charge losses. These coefficients are used to derive the energy of events when the trap correction is applied by the the software task XRTCALPI.

launch.

### C.1 Photon Counting mode trap mapping

In Photon Counting mode traps are mapped in the central 200x200 pixels window of the CCD, where most of the GRB afterglows and other astrophysical X-ray sources are observed by the XRT. The exact trap localisation ideally requires the collection of enough source events to fit the Si-K $\alpha$  line with a Gaussian for each CCD pixel. This isn't feasible, as it would greatly exceed the allocated calibration observing time of the *Swift* mission. In practice, the exposure times of the Cas A and Tycho calibration observations are sufficient to obtain an acceptable Gaussian fit of the Si-K $\alpha$  line from the merging of events of 20 adjacent pixels. Software tools have been developed to fit the Si-K $\alpha$  line along the CCD columns, to localise traps and measure their depths. An example of trap mapping and correction is shown in Figure C.6. A trap  $\simeq 100$  eV

Cas A spectral degradation 2005 vs 2010

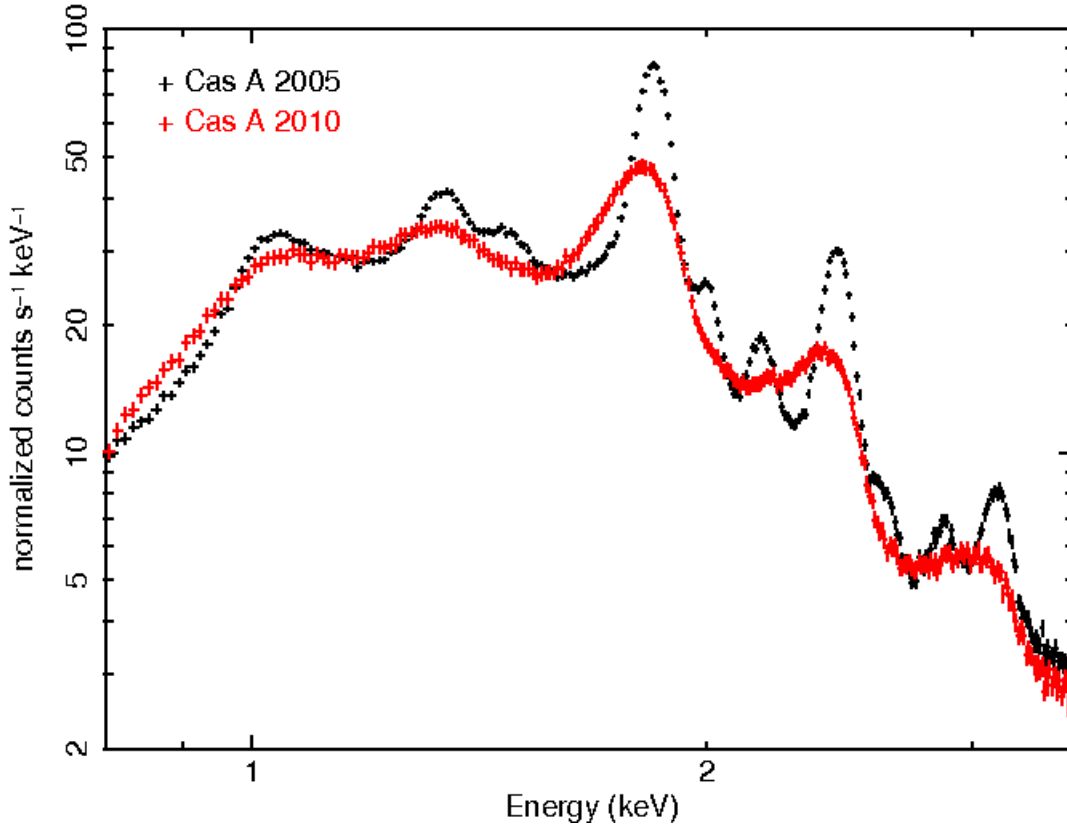


Figure C.5: Comparison of the Windowed Timing mode Cas A spectrum at launch and in a 2010 observation, showing the reduced energy resolution that causes the broadening of the brighter lines of the remnant and the complete disappearance of the weaker lines. The fit of the Silicon K  $\alpha$  line with an asymmetric Gaussian in IDL yielded an FWHM of  $103 \pm 3$  eV and of  $259 \pm 37$  eV, in the 2005 and 2010 dataset respectively.

deep is localised in Column DETX = 256, at the approximate row coordinate DETY = 310. In the top plot, each datapoint is the energy centroid of the Gaussian fit of events collected in the 20 pixels above the DETY row coordinate. The line centroid energy after the correction for trap losses has been applied is shown in the bottom plot. This technique allows the identification of traps with a depth of 20 eV or larger.

Figure C.7 is the comparison of the spectrum of the Tycho remnant observed in October 2009 and the spectrum after the correction for traps has been applied, showing an evident recovery of the spectral lines and of the energy resolution. To quantify the improvement in resolution the Si-K $\alpha$ , S-K $\alpha$  and Fe-K $\alpha$  lines of the observed and the corrected spectra of different calibration epochs were fitted in IDL with a modified Gaussian ( $f \propto e^{-\frac{(x-E)^2}{2\sigma_1^2}}$  for  $x \geq E$ ,  $f \propto e^{-\frac{(x-E)^2}{2\sigma_2^2}}$  for  $x < E$ ), needed to model the asymmetric distortion of the spectral lines caused by trap losses. The results are reported in Table 2.

Trap mapping of the central window of the CCD requires a substantial investment of observing time. Outside the central 200x200 pixels, to keep the exposure time within the allocated calibration time budget, shorter observations of the SNRs are collected, allowing the measurement of the cumulative charge losses due to traps in specific columns (column energy offsets). This approach, that doesn't localise and correct for the charge losses of individually trapped pixels,

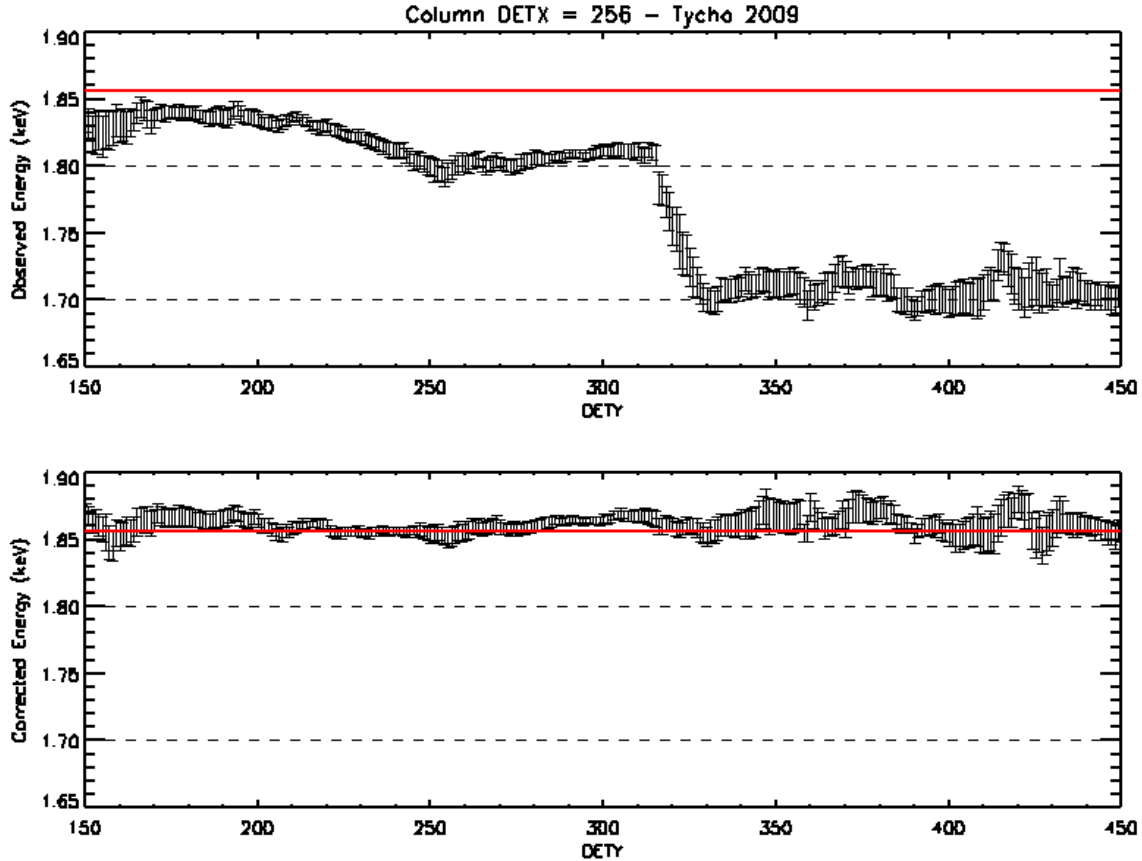


Figure C.6: In the top plot, a deep trap is identified in a Cas A Photon Counting mode observation in CCD column DETX=256 at DETY  $\sim$  310; in the bottom plot, the Si-K $\alpha$  line energy is restored after the trap correction has been applied.

provides nevertheless a considerable improvement of the energy resolution.

The serial CTI coefficient is defined as the fraction of charge lost per pixel during serial transfers, when the charge is readout in the serial register to the output amplifier. In reality, the CTI is not uniform over the detector because of the non-uniform distribution of traps. The measurement of the columns energy offsets is in effect a more precise characterisation of the serial charge losses than the CTI coefficient, because it evaluates the charge lost for each column. Hence, the serial CTI coefficient GC1\_TRAP has been set to zero in the current release.

## C.2 Windowed Timing mode trap mapping

Windowed Timing mode provides high time resolution with 1-D spatial localisation, therefore it is not possible to measure the row coordinates and depths of single traps. For this reason, global energy offsets from the reference Si-K $\alpha$  line are measured on a column by column basis, as in PC observations outside the central 200x200 pixels window.

The *Swift-XRT* pipeline can estimate the *average* row coordinate of a source observed in WT mode if the Right Ascension and the Declination of the target are specified when processing the data. To take advantage of the estimated source average row coordinate for trap mapping purposes, in the latest round of calibration observations Tycho was observed in WT mode

Tycho 2009 PC mode – Observed and Corrected Spectra

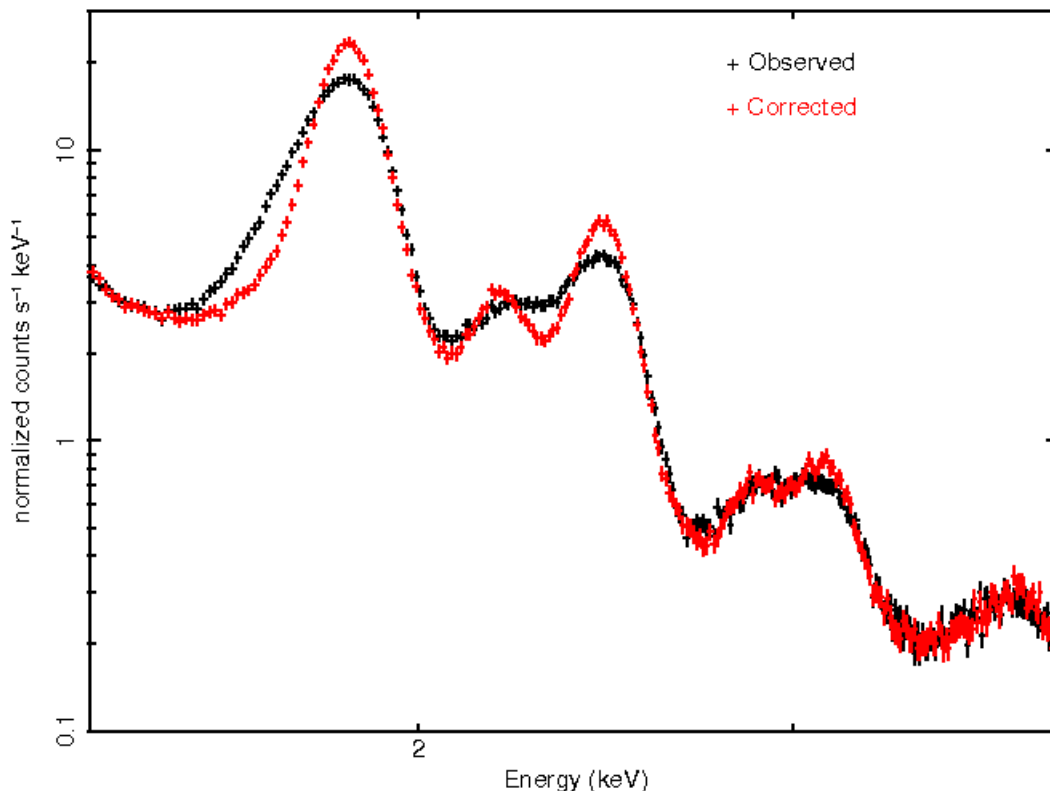


Figure C.7: Comparison of the observed and the trap corrected spectra extracted from a PC mode observation of the Tycho SNR from October 2009. The fit of the Silicon  $K\alpha$  line with an asymmetric Gaussian in IDL yielded a FWHM of  $179 \pm 8$  eV for the observed spectrum and of  $132 \pm 3$  eV for the corrected spectrum.

at three offsets pointings, at the average CCD row positions DETY=100, DETY=300 and DETY=500, allowing the derivation of the energy offsets of three segments of each column (from DETY=[1,200], DETY=[201,400] and DETY=[401,600]). It is therefore recommended to specify the source's RA and Dec when running the *Swift-XRT* pipeline to obtain the best possible energy resolution in Windowed Timing mode.

Table 3 reports the FWHM values of the Si- $K\alpha$ , S- $K\alpha$  and Fe- $K\alpha$  lines of the observed and the corrected WT spectra at different epochs, fitted in IDL with an asymmetric Gaussian. Figure C.8 compares the observed and corrected WT spectra of Cas A taken in October of 2007.

### C.3 Trap offsets Energy dependence

The traps energy offset is a function of the incident photon energy. The energy dependence is modelled in the gain files with a broken power law (equation A.18). The Sulfur and Iron lines in Cas A and Tycho are used to derive the energy dependence above the break, while observations of the SNR E0102 with emission lines between 0.5 and 1 keV were used below the break.

The observed and trap-corrected spectrum of the SNR E0102 used for this analysis is shown in

Cas A 2007 WT mode – Observed and Corrected Spectra

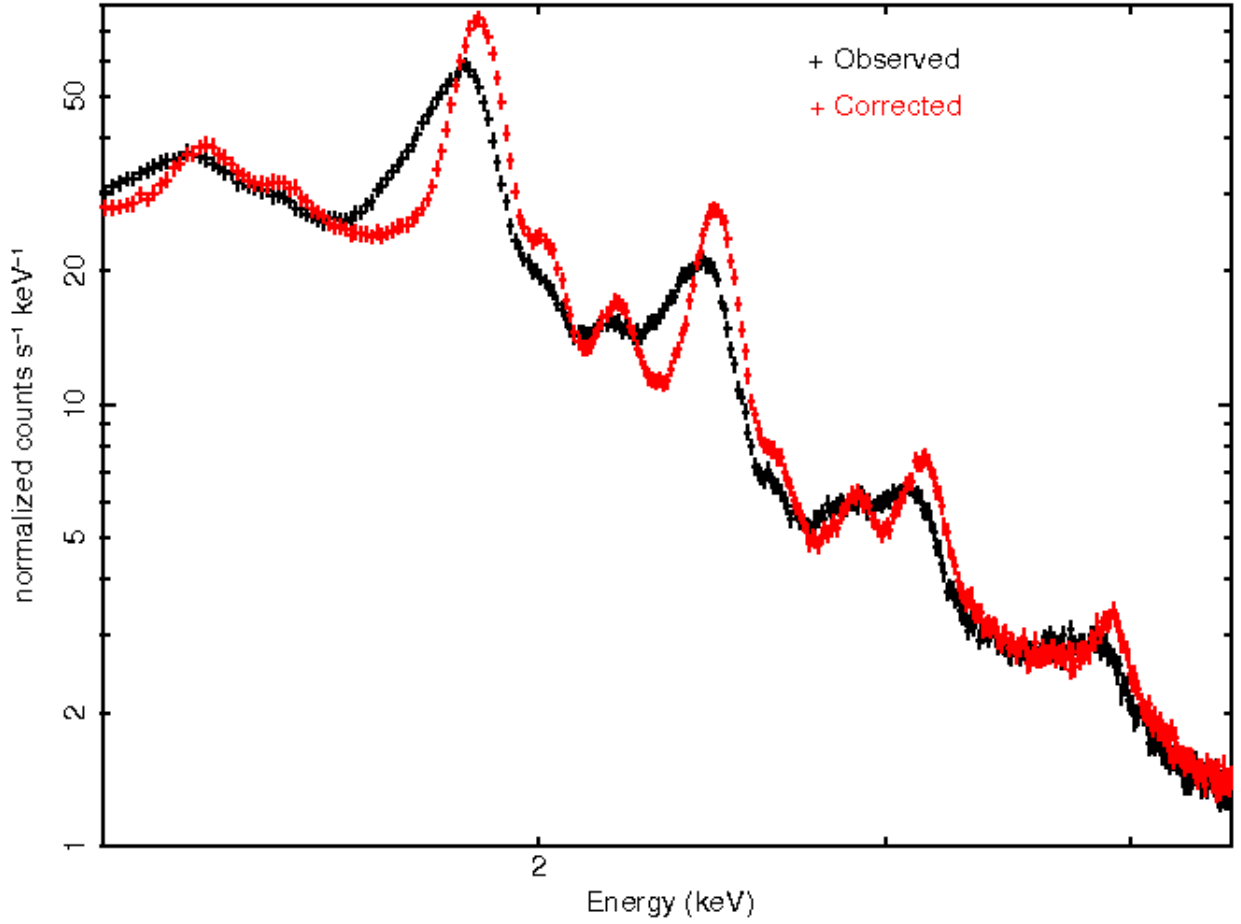


Figure C.8: Comparison of the observed and the trap corrected spectra extracted from WT observations of the Cas A SNR in October of 2007. The fit of the Silicon  $K\alpha$  line with an asymmetric Gaussian in IDL yielded a FWHM of  $152 \pm 13$  eV for the observed spectrum and of  $106 \pm 3$  eV for the corrected spectrum.

Figure C.9. PC mode observations yielded  $\alpha_1 = 0.80$  and  $\alpha_2 = 0.80$  before 2011 and  $\alpha_1 = 0.80$  and  $\alpha_2 = 0.85$  since 2011, with the break set at the reference energy of 1.856 keV; for WT mode observations before 2011, the measured slopes are  $\alpha_1 = 0.70$  and  $\alpha_2 = 0.50$ , since 2011 the slopes are  $\alpha_1 = 0.80$  and  $\alpha_2 = 0.50$ , with the break set to 3.0 keV.

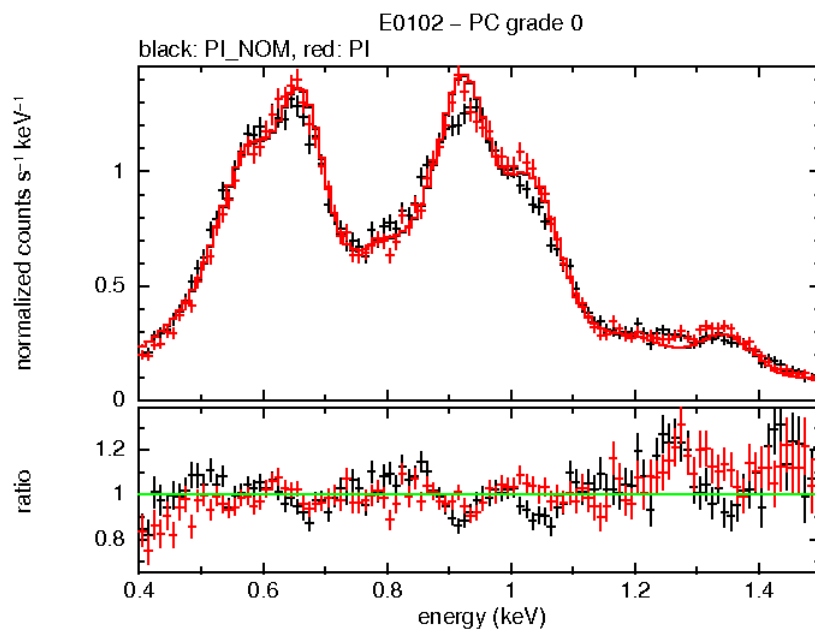


Figure C.9: Observed (black) and trap-corrected (red) spectrum of E0102 used to determine the CTE energy dependence at low energies. Dataset from 2008 to 2010 were merged to extract the spectra, and grade 0 events were selected. There is a definite improvement of the lines around 0.675, 0.915 and 1.035 keV in the trap corrected spectrum.

## D Previous Releases

Table D.1: Previous gain file releases.

FILENAME	VALID DATE	RELEASE DATE	REVISION
swxpcgain20010101v003.fits	01-Jan-2001	15-Oct-2004	003
swxpdgain20010101v003.fits	01-Jan-2001	15-Oct-2004	003
swxwtgain20010101v003.fits	01-Jan-2001	15-Oct-2004	003
swxpcgain20010101v004.fits	01-Jan-2001	10-Jan-2005	004
swxpdgain20010101v004.fits	01-Jan-2001	10-Jan-2005	004
swxwtgain20010101v004.fits	01-Jan-2001	10-Jan-2005	004
swxpcgain20010101v005.fits	01-Jan-2001	12-Oct-2005	005
swxpdgain20010101v005.fits	01-Jan-2001	12-Oct-2005	005
swxwtgain20010101v005.fits	01-Jan-2001	12-Oct-2005	005
swxpcgain20010101v006.fits	01-Jan-2001	1-Dec-2005	006
swxpdgain20010101v006.fits	01-Jan-2001	1-Dec-2005	006
swxwtgain20010101v006.fits	01-Jan-2001	1-Dec-2005	006
swxpcgains0_20010101v007.fits	01-Jan-2001	30-Jul-2007	007
swxpcgains6_20010101v007.fits	01-Jan-2001	30-Jul-2007	007
swxpdgains0_20010101v007.fits	01-Jan-2001	30-Jul-2007	007
swxwtgains0_20010101v007.fits	01-Jan-2001	30-Jul-2007	007
swxwtgains6_20010101v007.fits	01-Jan-2001	30-Jul-2007	007
swxwtgains0_20010101v008.fits	01-Jan-2001	21-Apr-2008	008
swxwtgains6_20010101v008.fits	01-Jan-2001	21-Apr-2008	008
swxpcgains0_20010101v008.fits	01-Jan-2001	07-Apr-2009	009
swxwtgains0_20010101v009.fits	01-Jan-2001	07-Apr-2009	009
swxpdgains0_20010101v008.fits	01-Jan-2001	07-Apr-2009	009
swxpcgains6_20010101v008.fits	01-Jan-2001	07-Apr-2009	009
swxwtgains6_20010101v009.fits	01-Jan-2001	07-Apr-2009	009
swxpcgains6_20010101v009.fits	01-Jan-2001	01-Dec-2009	009
swxwtgains6_20010101v010.fits	01-Jan-2001	01-Dec-2009	009
swxpcgains6_20010101v010.fits	01-Jan-2001	07-Jun-2011	010
swxwtgains6_20010101v011.fits	01-Jan-2001	07-Jun-2011	010
swxpcgains0_20010101v009.fits	01-Jan-2001	07-Jun-2011	010
swxwtgains0_20010101v010.fits	01-Jan-2001	07-Jun-2011	010
swxpdgains0_20010101v009.fits	01-Jan-2001	07-Jun-2011	010
swxpcgains6_20010101v011.fits	01-Jan-2001	09-Feb-2012	011
swxwtgains6_20010101v012.fits	01-Jan-2001	09-Feb-2012	011
swxpcgains0_20010101v010.fits	01-Jan-2001	09-Feb-2012	011
swxwtgains0_20010101v011.fits	01-Jan-2001	09-Feb-2012	011
swxpdgains0_20010101v010.fits	01-Jan-2001	09-Feb-2012	011

Table D.1 lists the gain files made available through previous releases of the *Swift*-XRT CALDB and are described in CALDB documents SWIFT-XRT-CALDB-04\_v11, SWIFT-XRT-CALDB-04\_v10, SWIFT-XRT-CALDB-04\_v9, SWIFT-XRT-CALDB-04\_v8, SWIFT-XRT-CALDB-04\_v2 and SWIFT-XRT-CALDB-04.